Clays and Clay Minerals, Vol. 53, No. 2, 147–154, 2005.

ATOMIC FORCE MICROSCOPY STUDY OF MONTMORILLONITE DISSOLUTION UNDER HIGHLY ALKALINE CONDITIONS

SHINGO YOKOYAMA[1], MASATO KURODA[1] AND TSUTOMU SATO[2,*]

[1] Graduate School of Natural Science and Technology, Kanazawa University, Kakuma, Kanazawa, Ishikawa 920-1192, Japan
[2] Institute of Nature and Environmental Technology, Kanazawa University, Kakuma, Kanazawa, Ishikawa 920-1192, Japan

Abstract—Montmorillonite dissolution under highly alkaline conditions (pH = 13.3; I = 0.3 M) was investigated by bulk dissolution methods and *in situ* atomic force microscopy (AFM). In bulk dissolution experiments, initial SiO_2 concentrations were high, and a steady state was reached after 136 h. The dissolution rates derived from the edge surface area (ESA) at the steady-state condition at 30, 50 and 70ºC were 3.39×10^{-12}, 1.75×10^{-11} and 5.81×10^{-11} mol/m^2 s, respectively. The AFM observations were conducted under three conditions: (Run I) short-term *in situ* batch dissolution at RT; (Run II) long-term *in situ* flow-through dissolution at RT; and (Run III) long-term batch dissolution at 50ºC. The observed reductions in montmorillonite particle volume for Runs I and II were due primarily to edge-surface dissolution. The ESA-based dissolution rate for Run I (10^{-9} mol/m^2 s) was three orders of magnitude faster than that for Run II (10^{-12} mol/m^2 s). The rate obtained for Run II corresponded to the rate at the steady-state conditions in the bulk dissolution experiments. A small number of etch pits developed in Run III slightly increased the ESA of montmorillonite since most of the montmorillonite particles were separated into monolayers lacking three-dimensional periodicity. The ESA-based dissolution rate for Run III was 2.26×10^{-11} mol/m^2 s. Dissolution rates based on long-term AFM observations could be directly compared with steady-state rates obtained from bulk dissolution experiments. The AFM observations indicated that dissolution occurred at edge surfaces; therefore, the ESA should be used to calculate the dissolution rate for montmorillonite under alkaline conditions. Dissolution rates of individual particles with different morphologies estimated by AFM were similar to rates estimated from bulk dissolution experiments.

Key Words—Alkaline Conditions, Atomic Force Microscopy, Dissolution Rate, Montmorillonite, Reactive Surface Area.

INTRODUCTION

The extensive use of smectite-rich bentonite as a buffer material in radioactive waste disposal is largely due to the suitable properties of smectites. However, smectites are dissolved by the highly alkaline pore-water produced by the interaction of local groundwater with concrete (pH 13–13.5; Atkinson, 1985), and the dissolution may diminish the bentonite's desirable properties, such as its physical and chemical buffering capacity. Therefore, the interaction between smectite and highly alkaline pore-water has become a major consideration in assessing the performance of bentonites in radioactive waste disposal.

Bulk dissolution experiments have been used to study the dissolution behavior of smectites under alkaline conditions (Hayashi and Yamada, 1990; Bauer and Berger, 1998; Bauer and Velde, 1999; Taubald *et al*., 2000; Cama *et al*., 2000; Huertas *et al*., 2001; Rassineux *et al*., 2001; Claret *et al*., 2002). Such experiments involve the measurement of solvent concentrations in output solutions, and the concentrations are then correlated with the dissolution mechanism and rates. Dissolution rates (mol/m^2 s) are usually derived from specific surface areas determined by the N_2-BET method. However, some authors are skeptical about this practice since the N_2-BET surface area does not necessarily correspond to the reactive surface area during the dissolution reaction (Rufe and Hochella, 1999; Bosbach *et al*., 2000; Bickmore *et al*., 2001; Gautier *et al*., 2001; Brandt *et al*., 2003; Tournassat *et al*., 2003).

In situ observation by AFM permits determination of the reactive surface and derivation of dissolution rates on the order of 10^{-6}–10^{-10} mol/m^2 s (Dove and Chermak, 1994; Dove and Platt, 1996). The effect of differences in particle morphology and size on the dissolution behavior of smectites can also be determined by AFM. However, *in situ* AFM studies are limited for smectite because smectite dissolution rates are extremely slow. *In situ* AFM studies have therefore been conducted at extremely low pH (*e.g.* Bosbach *et al*., 2000; Bickmore *et al*., 2001). So far, no experiments have been performed under highly alkaline conditions.

Bosbach *et al*. (2000) performed one of the most notable *in situ* AFM experiments and concluded that hectorite dissolves along the edge surfaces under acidic conditions (pH = 2 at 22ºC). The edge surface area

* E-mail address of corresponding author:
tomsato@earth.s.kanazawa-u.ac.jp
DOI: 10.1346/CCMN.2005.0530204

Copyright © 2005, The Clay Minerals Society

https://doi.org/10.1346/CCMN.2005.0530204 Published online by Cambridge University Press

(ESA) used to calculate the dissolution rate ($R = 7.3 \times 10^{-9}$ mol/m^2 s) was also determined by AFM. However, their observations were carried out only for several hours, and the rate they obtained cannot be compared directly with the dissolution rate obtained from a bulk dissolution experiment conducted for several days. Brandt *et al*. (2003) have used a combined microscopic (*in situ* observation using AFM) and macroscopic (mixed flow experiments) approach. It was shown that dissolution rates obtained by using the reactive surface area agree well for both microscopic and macroscopic experiments. In this study, a similar approach has been used to elucidate and compare the dissolution behavior of smectites under highly alkaline conditions in bulk and microscopic experiments.

We observed the dissolution behavior of montmorillonite under alkaline condition using *in situ* AFM, and compared the results with those of bulk dissolution experiments. Our major goals were (1) to determine the reactive surfaces and dissolution rate of montmorillonite under alkaline condition and (2) to explain the change in solvent SiO_2 concentration with time in the bulk dissolution experiments in terms of the change in montmorillonite particle volume as detected by AFM.

MATERIALS AND METHODS

Starting material

Refined montmorillonite (Kunipia-P, Kunimine Industry Co. Ltd) from a Na-type bentonite deposit in Yamagata Prefecture, Japan, was used. This bentonite is a candidate for use as a buffer material surrounding the iron seal overpack in the underground disposal of high-level radioactive waste in Japan.

The sample was checked for purity by X-ray diffraction (XRD) analysis (Rigaku RINT 1200). No other constituents were identified in the XRD pattern after ethylene glycol treatment. The structural formula of the sample as calculated from X-ray fluorescence (XRF) analysis is as follows:

$$Na_{0.39}K_{0.01}Ca_{0.06}(Al_{1.56}Mg_{0.33}Fe_{0.09}Ti_{0.01})(Si_{3.87}Al_{0.13})O_{10}(OH)_2.$$

The sample was identified as montmorillonite with Al substitution for Si in the tetrahedral sheet (*i.e*. beidellitic component).

Dissolution experiments

Bulk dissolution experiments. A flow-through system consisting of tall cylindrical stirred-flow Teflon reactors was employed. Ionic strength was fixed using a 0.3 M NaOH solution (pH 13.3±0.1), and the flow rate was maintained at a constant 0.2 mL/min. A 120 mg sample was added to 120 mL of solution inside the reactor. The resulting suspension was stirred magnetically with a Teflon-coated stirring bar to prevent settling and flocculation of the clay particles. The reactors were fully immersed in a water bath to maintain a constant temperature of 30, 50 or 70±1.0ºC. The reaction period was ~7 days. Preparation and storage of stock solutions, measurement of pH, and sampling of output solutions were carried out in an N_2-filled glove box to avoid solution pH changes caused by interaction of the solution with atmospheric CO_2. A peristaltic pump was used to transfer the reactant solutions from their containers to the reaction vessels and from the reaction vessels to the collecting containers. The SiO_2 content in the collected filtrate was determined by UV-visible spectrometry using the molybdate blue method.

Specific surface areas for calculation of dissolution rates were obtained using the three-point N_2 adsorption isotherms (N_2-BET) and observations by AFM. In the N_2-BET method, samples were degassed for 12 h at 300ºC. Before the measurements were conducted, the samples were treated with a 0.3 M NaCl or NaOH solution at 25ºC for 2 days. After treatment, an HCl solution was added to the NaOH suspension until it reached pH 9. The samples were then washed with 80% ethanol until the pH value became constant and the samples were chloride-free (as indicated by the $AgNO_3$ test). The samples were then freeze dried.

Dissolution experiments observed by AFM. Samples used in the observations by AFM were prepared by the following technique. A 10 mg sample was added to 100 mL of deionized water and dispersed ultrasonically for 30 min. The resulting suspension was placed on a mica substrate and left for 20 min. Excess suspension was taken up with filter paper, and the mounted samples were air dried at room temperature (25ºC). The procedure developed by Bickmore *et al*. (1999) to fix the samples on the mica substrate was not followed due to differences in experimental conditions (*i.e*. pH 13.3). The pyramidal Si_3N_4 tips used in the AFM (JEOL JSTM-4200D) imaging were set at contact mode at capture times ranging from 30 to 90 s per image. Surface areas of montmorillonite particles were calculated using the *WinSPM DPS* Version 2.01 (JEOL Ltd.) and *Canvas* Version 9.0.2 (ACD Systems of America Inc.). In *Canvas*, surface area measurements were performed by digitizing the boundary of each particle. The analytical error in ten area measurements of the same particle is within 1%.

Three types of AFM experiments were performed: (Run I) short-term *in situ* batch dissolution experiment at room temperature (25ºC); (Run II) long-term *in situ* flow-through dissolution experiment at room temperature (25ºC); and (Run III) long-term batch dissolution experiment at 50ºC. All the dissolution experiments were conducted under highly alkaline conditions (pH 13.3±0.1) using 0.3 M NaOH solutions. The samples were placed inside the AFM fluid cell, which was filled with a 0.3 M NaOH solution (Run I); and a constant flow rate (0.1 mL/min) was maintained during

https://doi.org/10.1346/CCMN.2005.0530204 Published online by Cambridge University Press

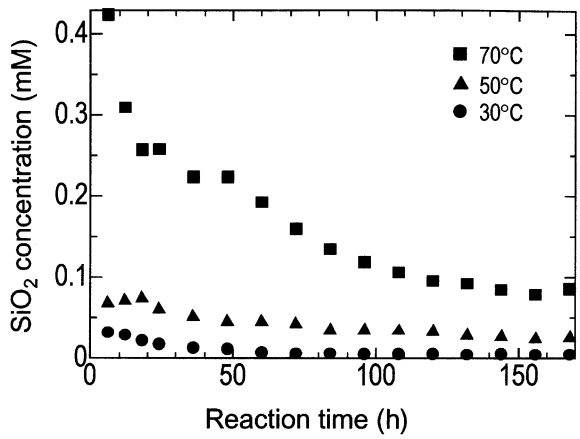


Figure 1. SiO_2 concentrations (mM) in the output solution during the bulk dissolution experiments. SiO_2 concentrations reached a steady state after 136 h.

the flow-through experiment (Run II). The flow of NaOH solution to the fluid cell was stopped briefly only during the AFM imaging process so that good images could be obtained. The stock solutions were prepared and stored inside an N_2-filled glove box. For Run III, the samples mounted on mica plates were immersed and heated at 50ºC in 50 mL of 0.3 M NaOH solution inside Teflon containers. The dissolution reactions were allowed to proceed for 6 to 33 days at 50ºC; after the reaction period, the samples were placed inside the fluid cell of the AFM filled with 0.3 M NaCl solution to prevent further dissolution with the entrained alkaline solution. The montmorillonite samples mounted on the mica plate were observed by AFM at 25ºC to detect changes in particle volume after the dissolution reactions. 100 particles were evaluated so that the results would be statistically viable.

RESULTS AND DISCUSSION

Dissolution rates from bulk dissolution experiments

In the bulk dissolution experiments, high concentrations of dissolved SiO_2 were observed during the initial stages of the reaction. The SiO_2 concentrations reached a steady state after 136 h (Figure 1), and the steady-state concentration increased with temperature: $[SiO_2]_{30°C} < [SiO_2]_{50°C} < [SiO_2]_{70°C}$ (Table 1).

Based on a simple mass balance equation, the dissolution rates (mol/m^2 s) in flow-through experiments are obtained from the following equation (Cama *et al*., 2000):

$$R = C_{SiO_2}\, q/A\, v_{SiO_2} \quad (1)$$

where C_{SiO_2} is the concentration of SiO_2 in the output solution (mol/L), v_{SiO_2} is the stoichiometric coefficient of SiO_2 in the dissolution reaction, A is the reactive surface area (m^2), and q is the fluid volume flux (flow rate) through the system (L/s). Dissolution rates calculated with equation 1 are shown in Table 1 which also lists the reactive surface areas used in calculating the rates: the N_2-BET surface area for the NaCl-treated sample (N_2-BET (A)) and the NaOH-treated sample (N_2-BET (B)), the total surface area (TSA), and the ESA measured by AFM. Dissolution rates generally increased with temperature, and they varied by two orders of magnitude depending on the surface area used in the calculation.

The dissolution rates obtained in previous studies were based on N_2-BET surface areas (Bauer and Berger, 1998; Bauer and Velde, 1999; Taubald *et al*., 2000; Cama *et al*., 2000; Huertas *et al*., 2001). In this study, the N_2-BET surface area of the NaOH-treated sample was three times larger than the N_2-BET surface area of the NaCl-treated sample. These results indicate that the N_2-BET surface area is easily affected by differences in sample preparation (chemical and physical). Therefore, the sample pretreatment for bulk dissolution studies will affect the dissolution rates calculated from N_2-BET surface areas.

Because AFM surface area measurements are unaffected by the aggregation effect observed in bulk methods, the ESA and basal surface area (BSA) can be determined. The TSA is the sum of the edge and double basal surface areas measured by the AFM method. The TSA determined in this study (781.0 m^2/g) was nearly equivalent to the TSA of the Wyoming montmorillonite (800 m^2/g) used by Sposito (1984) and Na-MX80 (788 m^2/g) summarized by AFM observations and low-pressure gas adsorption experiments in Tournassat *et al*. (2003). The ESA determined in this study (5.3 m^2/g) was slightly smaller than the value for Na-MX80 (8 m^2/g) (Tournassat *et al*., 2003), which can be attributed to differences in particle size. Hence, the ESA of each

Table 1. Steady-state SiO_2 concentrations and dissolution rates based on various surface areas.

Temperature (ºC)	SiO_2 concentration (mM)	Dissolution rate (mol/m^2 s)			
		N_2-BET (A)	N_2-BET (B)	TSA*	ESA*
30	0.005	2.33×10^{-12}	8.44×10^{-13}	2.30×10^{-14}	3.39×10^{-12}
50	0.026	1.20×10^{-11}	4.35×10^{-12}	1.19×10^{-13}	1.75×10^{-11}
70	0.086	4.00×10^{-11}	1.45×10^{-11}	3.94×10^{-13}	5.81×10^{-11}

N_2-BET (A): 7.7 m^2/g; N_2-BET (B): 21.3 m^2/g; TSA: 781.0 m^2/g; ESA: 5.3 m^2/g. The errors in surface-area measurements by N_2-BET method are generally ±10%. * Standard errors in TSA and ESA are ±0.2 and ±0.2 m^2/g, respectively.

https://doi.org/10.1346/CCMN.2005.0530204 Published online by Cambridge University Press

individual smectite sample used in dissolution experiments should be determined, as Tournassat *et al*. (2003) have previously suggested.

In situ AFM observations for montmorillonite dissolution at RT

In a short-term *in situ* batch dissolution experiment observed by AFM (Run I), the height of the observed montmorillonite particle (~15 Å) was close to the height of a single hydrated montmorillonite layer with two water layers between the montmorillonite layer and the mica substrate. This particle height remained constant during the observation period. The change in the particle volume brought about by the dissolution reaction is reflected in the change in the BSA (Figure 2). The general shape of the particle did not change significantly. Using an unpaired t-test, the difference between the initial (Figure 2a) and final (Figure 2b) BSA indicated a significant difference with probability (P) = 2.09×10^{-105}. The linear decrease in the average BSA without the formation of etch pits suggests that the edge surface was the reactive site (Figure 2c).

The dissolution rate was obtained from the following equation:

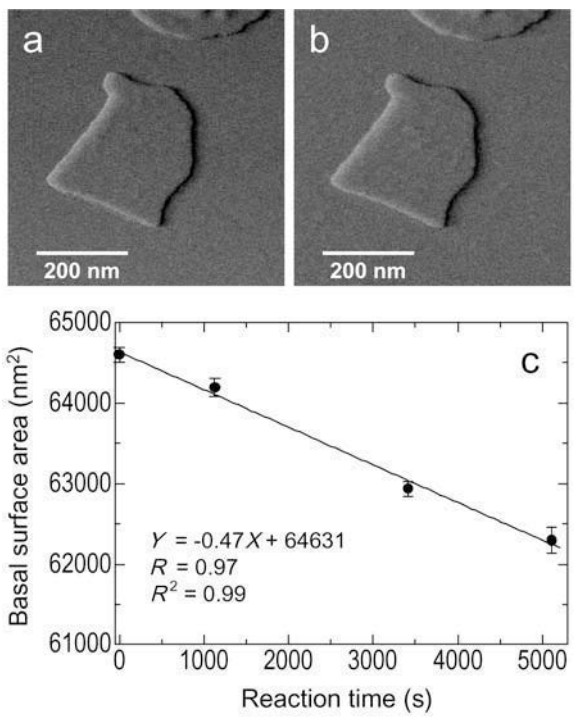


Figure 2. AFM images of a montmorillonite particle in a pH 13.3 aqueous solution at 25ºC (a) after 0 min and (b) after 87 min. (c) Basal surface area of montmorillonite particle during the short-term *in situ* batch dissolution experiment (Run I). The standard errors on BSA estimates are based on ten repeated measurements of the same particle. R and R^2 indicate the coefficient of correlation and determination at regression line of average BSA, respectively.

$$R = d_{BSA}/(U_{mont} \cdot N \cdot A) \quad (2)$$

where d_{BSA} is the change in the BSA with reaction time (nm^2/s), U_{mont} is the *ab* unit-cell area of montmorillonite (nm^2), N is Avogadro's constant and A is the reactive surface area (m^2). The value for U_{mont} (0.46 nm^2) reported by MacEwan (1961) was used in the calculations. Results of the dissolution-rate calculations using the ESA (*i.e*. the reactive surface area) values before and after the dissolution reaction are listed in Table 2. The ESAs were calculated using the circumference of the particle and a height of 0.955 nm (as reported in Tournassat *et al*., 2003) for the dehydration of smectite. The dissolution rates calculated from the initial and final ESA values were similar. Surface area change during the dissolution reaction did not influence the dissolution rate observed for short-term dissolution reaction (*i.e*. reaction lasting several hours).

The observed particles were mostly dispersed monolayers, but some particles formed stacks as shown in Figure 3. The effect of particle morphology on the dissolution rate was illustrated more clearly in the long-term *in situ* AFM observations.

Estimation of AFM mechanical error during the long-term *in situ* AFM observations was necessary for estimating the BSA and circumference of the particle. This was performed by assuming the distances between the particles A, 1, 2 and 3 in Figure 3b to be constant. The AFM mechanical error was then estimated by determining the drift in these distances after 2, 4 and 8 days of the observations where a maximum of 7% error was detected. The measured BSAs and circumferences of particles after 4 and 8 days of observations were compensated for these mechanical errors. The general shape of referenced particles did not change significantly. An unpaired t-test was used to detect the difference between initial (2 days) and final (8 days) BSAs of observed particles which indicated significant differences with a range of probability (P) = 3.14×10^{-3} to 2.87×10^{-65}. The slight decrease in average BSA that occurred without the formation of etch pits suggests that edge surfaces were the reactive sites in the long-term dissolution observations. The dissolution rates calculated for each type of particle based on the initial ESAs were similar (Figure 3). Particle size, particle morphology (*i.e*. shape or rough particle face; black and white symbols), and the stacking of layers (circle and pyramidal symbols) did not

Table 2. Reactive surface areas and dissolution rates for short-term *in situ* batch dissolution experiment (Run I).

	Initial	Final
Reactive surface area* (nm^2)	999	982
Dissolution rate (mol/m^2 s)	1.68×10^{-9}	1.71×10^{-9}

* Standard errors in initial and final reactive surface area are ±5 and ±7 nm^2, respectively.

https://doi.org/10.1346/CCMN.2005.0530204 Published online by Cambridge University Press

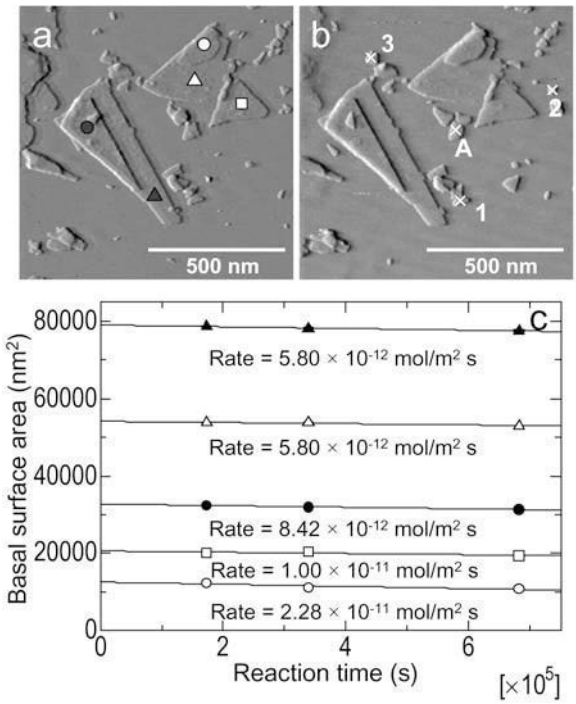


Figure 3. AFM images of montmorillonite particles in a pH 13.3 aqueous solution at 25ºC (a) after 2 days and (b) after 8 days. (c) Basal surface areas of montmorillonite particles during the long-term *in situ* flow-through dissolution experiment (Run II). Standard errors were calculated based on ten repeated measurements of the same particle.

profoundly affect dissolution rates in this observation range. This is evident in the calculated dissolution rates of different montmorillonite particles which were approximately constant since the ESAs exposed to the reacting solution, *i.e.* the surface where the dissolution occurred, were used in the calculations.

The dissolution rate recalculated to 25ºC from the results of bulk dissolution experiments ($R = 2.56 \times 10^{-12}$ mol/m^2 s) was three orders of magnitude slower than the dissolution rate derived from the results of Run I. If the particle in Run I dissolved at this rate (*i.e.* $R = 2.56 \times 10^{-12}$ mol/m^2 s), particle change cannot be detected by the AFM during the reaction period of Run I (*i.e.* 0.006% BSA change). The dissolution rates obtained in Run II approximated the dissolution rate recalculated to 25ºC from the results of bulk-dissolution experiments.

Dissolution behavior of montmorillonite under alkaline conditions

In the bulk-dissolution experiments, a high SiO_2 concentration in the output solutions was observed in the initial stages (up to 100 h). The SiO_2 concentration decreased continuously with time and reached a constant rate in the later stages of the dissolution reaction (after 136 h). This trend has also been observed in other mineral dissolution studies, associated with the dissolution of very small mineral particles, broken surfaces, or crystal defects on the mineral surfaces (Holdren and Berner, 1979; Schott *et al*., 1981; Chou and Wollast, 1984, 1985; Knauss and Wolery, 1988, 1989; Stillings and Brantley, 1995; Huertas *et al*., 1999; Bickmore *et al*., 2001; Brandt *et al*., 2003). The dominant influence on the observed dissolution trends cannot be determined by bulk dissolution experiments, but AFM observations in dissolution experiments do allow the discrimination of the factors that give rise to the observed dissolution trends.

We monitored the initial stages of the dissolution reaction by means of *in situ* AFM observations, and we determined a dissolution rate of ~10^{-9} mol/m^2 s (Run I). However, AFM observations indicated a very slow dissolution rate (10^{-12} mol/m^2 s) at later stages in the reaction (during the period from 2 to 8 days; Run II). This change of dissolution rate during the dissolution process seems to correspond to the changes in dissolved SiO_2 concentration from the bulk dissolution experiments. The changes in the solvent concentrations during bulk dissolution experiments were assumed to be due to change in the dissolution behavior of montmorillonite particles. The change of nontronite dissolution behavior during the dissolution process was discussed by Bickmore *et al*. (2001) who concluded through *in situ* AFM observations that dissolution fronts originating at broken edges or at crystal face defects would be quickly pinned at the (010), (110) and ($1\bar{1}0$) faces of nontronite crystals owing to their exceptional stability. Consequently, no observable dissolution along these faces would occur under acidic conditions. Similarly, montmorillonite dissolution under alkaline conditions could also occur. It has already been shown that different dissolution rates were obtained in short- and long-term dissolution experiments even when the reactive surface sites are the same (*i.e.* edge surfaces). In fact, the rate determined by short-term AFM observations does not correspond to the real dissolution rate of the mineral surface (*i.e.* constant rate at steady-state conditions), and only the result of long-term observations corresponds to the steady-state dissolution indicated in bulk dissolution experiments. Therefore, AFM observations for the calculation of a specific dissolution rate for smectite should be conducted at later stages of the reaction. Since the dissolution rate obtained from short-term observations shown by previous studies corresponds only to the initial stages, these rates are not comparable to the dissolution rates determined by bulk dissolution experiments corresponding to the later stages (*i.e.* steady-state conditions). Dissolution rates derived at longer observation periods using the *in situ* AFM method are directly comparable with the rates derived from bulk dissolution studies.

Long-term batch dissolution experiment at 50ºC (Run III)

The BSA and the thickness of individual particles after 6, 12, 19 and 33 days were observed by AFM.

https://doi.org/10.1346/CCMN.2005.0530204 Published online by Cambridge University Press

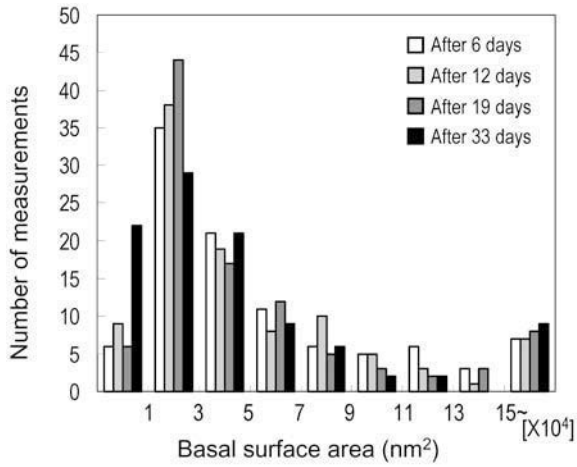


Figure 4. Distribution of the basal surface areas as measured by AFM during the long-term batch dissolution experiment at 50ºC (Run III). The number of small particles increased as the reaction progressed.

Particles with small BSAs (*i.e.* small particle size) are mostly dissolved after 33 days (the longest reaction time), and were not considered in this type of experiment. Furthermore, dissolution rates generally decrease when the small particles are considered in the calculation, and this decrease leads to an inaccurate estimate of the rate. Size limits for the particles were based on the dissolution rate determined by bulk dissolution experiment (at 50ºC) using the ESA. The estimated 33-day BSAs of individual particles in the 6, 12 and 19 day samples were calculated with equation 2. If the calculated BSA was negative, it was not used for the calculation of dissolution rate. Such particles would have dissolved completely before the longest reaction time (*i.e.* 33 days).

A histogram of the BSAs of montmorillonite particles after the dissolution reactions is shown in Figure 4. The number of small particles increased as the dissolution reactions progressed. The larger particles (with BSAs

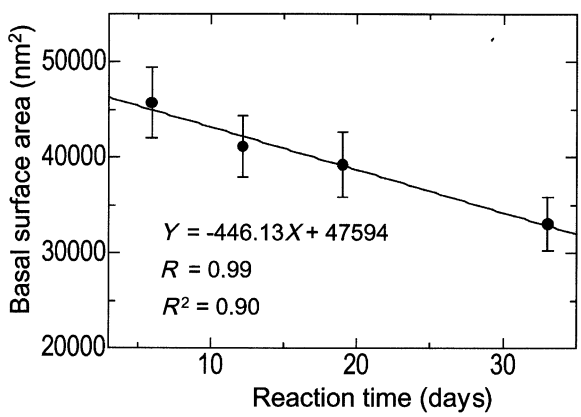


Figure 5. Basal surface area of montmorillonite particles during the long-term batch dissolution experiment at 50ºC (Run III). R and R^2 indicate the coefficient of correlation and determination at regression line of average BSA, respectively.

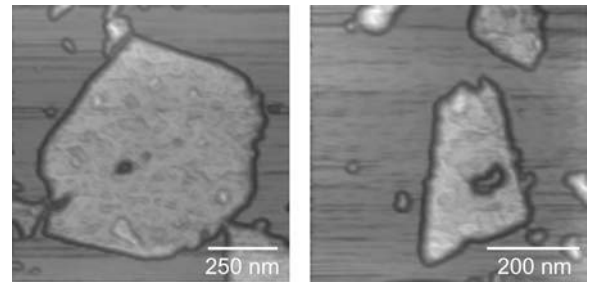


Figure 6. AFM images of montmorillonite particles with etch pits on the basal surface. These montmorillonite particles were observed after 12 days in the long-term batch dissolution experiment at 50ºC (Run III).

$>15 \times 10^4$ nm^2) would result from analytical errors due to their larger size modality (15×10^4 to 63×10^4 nm^2). As these larger particles do not reflect a decreasing BSA trend during the dissolution process, particles with sizes $>15 \times 10^4$ nm^2 were excluded. The differences between the initial (6 days) and final (33 days) BSAs of the observed particles were analyzed by an unpaired t-test, which indicated a significant difference with probability (P) = 3.49×10^{-3}. The variation in the average BSA values is plotted in Figure 5. The BSA decreased linearly from the steady-state conditions in the bulk dissolution experiments (6 days) to the end of the experiment (33 days).

Although etch pits formed on the basal surface of a few particles (Figure 6), they did not appear to be the dominant dissolution sites. This suggests that the reduction in particle volume was due mainly to dissolution along edge surfaces. The dissolution rates determined using the initial and final ESA values were calculated to be 2.26×10^{-11} and 2.58×10^{-11} mol/m^2 s, respectively (Table 3). The dissolution rates based on AFM observations were similar to the rate obtained from the bulk dissolution experiment at 50ºC as both observations were carried out until the steady-state condition was reached, and the reactive surface areas (*i.e.* ESAs) were used in calculating the dissolution rates.

Reactive surface in montmorillonite dissolution under highly alkaline conditions

In a recent study, Si–O–Al sites (on the edge surface) were the most important reactive sites in the dissolution reaction of dioctahedral phyllosilicates (Ganor *et al.*, 1995; Zysset and Schindler, 1996;

Table 3. Average reactive surface areas and dissolution rates for long-term batch dissolution experiment (Run III).

	Initial	Final
Reactive surface area* (nm^2)	820	719
Dissolution rate (mol/m^2 s)	2.26×10^{-11}	2.58×10^{-11}

* Standard errors in initial and final reactive surface area are ±36 and ±35 nm^2, respectively.

https://doi.org/10.1346/CCMN.2005.0530204 Published online by Cambridge University Press

Bickmore *et al*., 2001; Bickmore *et al*., 2003). Sites where Si has been substituted for Al in the tetrahedral sheet (beidellitic component) can also contribute to the dissolution reactions (Nagy, 1995). Etch pits on the basal surface were observed in Run III in which the sample used contained a beidellitic component. If the beidellitic component contributed to the dissolution reaction, more etch pits would have been observed on the basal surface. The presence of etch pits on some of the particles can be attributed to defective sites, which are also highly reactive (Nagy, 1995).

The formation and growth of etch pits in three-dimensional crystals (*e.g*. carbonate, quartz and feldspar) are important mechanisms in controlling the dissolution rate of minerals as the etch pits dissolve faster with depth as the dissolution reaction progresses (*e.g*. Gautier *et al*., 2001). For the montmorillonite used in this study, the formation of a small number of etch pits can be considered as contributing slightly to the increase in the edge surface area since most of the montmorillonite particles were separated into monolayers lacking three-dimensional periodicity. Consequently, we concluded that montmorillonite dissolution under highly alkaline conditions occurred primarily along edge surfaces at both the initial states and at later stages (*i.e*. at steady-state conditions).

When dissolution rates were calculated based on the ESAs, the rates of individual particles with different morphologies were similar to the rates estimated from bulk dissolution experiments. This similarity suggests that calculations of dissolution rates for montmorillonite under alkaline conditions should be based on the ESA, as Bosbach *et al*. (2000) and Bickmore *et al*. (2001) have previously reported using *in situ* observations of smectite dissolution under acidic condition.

CONCLUSIONS

Montmorillonite dissolution under alkaline conditions was investigated by means of both bulk and AFM dissolution experiments. *In situ* observations using AFM indicated that the dissolution of montmorillonite particles occurred primarily along edge surfaces from start to finish (Runs I and II). However, the dissolution rate at the initial stage (Run I, up to several hours) was three orders of magnitude faster than the rate at the steady-state condition (Run II). The dissolution rates obtained from long-term dissolution experiments using AFM (Runs II and III) agreed well with the rate obtained from bulk dissolution experiments. Therefore, AFM observations for the calculation of a specific dissolution rate for smectite should be conducted at steady-state conditions. Furthermore, the dissolution rates of individual particles calculated from the ESAs (*i.e*. the dominant reactive sites) were independent of particle morphology, size and stacking within the observation range.

ACKNOWLEDGMENTS

This study was supported financially by the Ministry of Economy and Industry, Japan; the Japan Atomic Energy Research Institute; the 21st century COE (Center of Excellence) program of the Japanese Ministry of Education, Culture, Science and Technology; and Kanazawa University, Japan. The authors express their utmost gratitude to Chelo S. Pascua (Kanazawa University) for help with the English.

REFERENCES

Atkinson, A. (1985) *The time-dependence of pH within a repository for radioactive waste disposal*. UKAEA Technical Report, AERE-R-11777, HMSO, London.

Bauer, A. and Berger, G. (1998) Kaolinite and smectite dissolution rate in high molar KOH solutions at 35º and 80ºC. *Applied Geochemistry*, **13**, 905–916.

Bauer, A. and Velde, B. (1999) Smectite transformation in high molar KOH solutions. *Clay Minerals*, **34**, 259–273.

Bickmore, B.R., Hochella, M.F., Jr., Bosbach, D. and Charlet, L. (1999) Methods for performing atomic force microscopy imaging of clay minerals in aqueous solutions. *Clays and Clay Minerals*, **47**, 573–581.

Bickmore, B.R., Bosbach, D., Hochella, M.F., Jr., Charlet, L. and Rufe, E. (2001) In situ atomic force microscopy study of hectorite and nontronite dissolution: Implications for phyllosilicate edge surface structures and dissolution mechanisms. *American Mineralogist*, **86**, 411–423.

Bickmore, B.R., Rosso, K.M., Nagy, K.L., Cygan, R.T. and Tadanier, C.J. (2003) Ab initio determination of edge surface structure for dioctahedral 2:1 phyllosilicates: Implications for acid-base reactivity. *Clays and Clay Minerals*, **51**, 359–371.

Bosbach, D., Charlet, L., Bickmore, B. and Hochella, M.F., Jr. (2000) The dissolution of hectorite: In-situ, real-time observations using atomic force microscopy. *American Mineralogist*, **85**, 1209–1216.

Brandt, F., Bosbach, D., Krawczyk-Bärsch, E., Arnold, T. and Bernhard, G. (2003) Chlorite dissolution in acid pH-range: A combined microscopic and macroscopic approach. *Geochimica et Cosmochimica Acta*, **67**, 1451–1461.

Cama, J., Ganor, J., Ayora, C. and Lasaga, A. (2000) Smectite dissolution kinetics at 80ºC and pH 8.8. *Geochimica et Cosmochimica Acta*, **64**, 2701–2717.

Chou, L. and Wollast, R. (1984) Study of the weathering of albite at room temperature and pressure with a fluidized bed reactor. *Geochimica et Cosmochimica Acta*, **48**, 2205–2217.

Chou, L. and Wollast, R. (1985) Steady-state kinetics and dissolution mechanism of albite. *American Journal of Science*, **285**, 963–993.

Claret, F., Bauer, A., Schäfer, T., Griffault, L. and Lanson, B. (2002) Experimental investigation of the interaction of clays with high-pH solutions: A case study from the Callovo-Oxfordian formation, Meuse-Haute Marne underground laboratory (France). *Clays and Clay Minerals*, **50**, 633–646.

Dove, P.M. and Chermak, J.A. (1994) Mineral-water interactions: fluid cell applications of scanning force microscopy. Pp 139–169 in: *Scanning Probe Microscopy of Clay Minerals* (K.L. Nagy, and A.E. Blum, editors). The Clay Minerals Society, Boulder, Colorado.

Dove, P.M. and Platt, F.M. (1996) Compatible real-time rates of mineral dissolution by atomic force microscopy (AFM). *Chemical Geology*, **127**, 331-338.

Ganor, J., Mogollón, J.L. and Lasaga, A.C. (1995) The effect of pH on kaolinite dissolution rates and on activation energy. *Geochimica et Cosmochimica Acta*, **59**, 1037–1052.

Gautier, J.-M., Oelkers, E.H. and Schott, J. (2001) Are quartz

https://doi.org/10.1346/CCMN.2005.0530204 Published online by Cambridge University Press

dissolution rates proportional to B.E.T. surface area? *Geochimica et Cosmochimica Acta*, **65**, 1059–1070.

Hayashi, H. and Yamada, M. (1990) Kinetics of dissolution of noncrystalline oxides and crystalline clay minerals in basic tiron solution. *Clays and Clay Minerals*, **38**, 308–314.

Holdren, G.R., Jr. and Berner, R.A. (1979) Mechanism of feldspar weathering. I. Experimental studies. *Geochimica et Cosmochimica Acta*, **43**, 1161–1171.

Huertas, F.J., Chou, L. and Wollast, R. (1999) Mechanism of kaolinite dissolution at room temperature and pressure Part II: Kinetic study. *Geochimica et Cosmochimica Acta*, **63**, 3261–3275.

Huertas, F.J., Caballero, E., Jimenez de Cisneros, C., Huertas, F. and Linares, J. (2001) Kinetics of montmorillonite dissolution in granitic solutions. *Applied Geochemistry*, **16**, 397–407.

Knauss, K.G. and Wolery, T.J. (1988) The dissolution kinetics of quartz as a function of pH and time at 70ºC. *Geochimica et Cosmochimica Acta*, **52**, 43–53.

Knauss, K.G. and Wolery, T.J. (1989) Muscovite dissolution kinetics as a function of pH and time at 70ºC. *Geochimica et Cosmochimica Acta*, **53**, 1493–1501.

MacEwan, D.M.C. (1961) Montmorillonite minerals. P. 143 in: *The X-ray Identification and Crystal Structure of Clay Minerals* (G. Brown, editor). Mineralogical Society, London.

Nagy, K.L. (1995) Dissolution and precipitation kinetics of sheet silicates. Pp. 173–233 in: *Chemical Weathering Rates of Silicate Minerals* (A.F. White, and S.L. Brantley, editors). Reviews in Mineralogy, **31**. Mineralogical Society of America, Washington, D.C.

Rassineux, F., Griffault, L., Meunier, A., Berger, G., Petit, S., Vieillard, P., Zellagui, R. and Munoz, M. (2001) Expandability-layer stacking relationship during experimental alteration of a Wyoming bentonite in pH 13.5 solutions at 35 and 60ºC. *Clay Minerals*, **36**, 197–210.

Rufe, E. and Hochella, M.F., Jr. (1999) Quantitative assessment of reactive surface area of phlogopite during acid dissolution. *Science*, **285**, 874–876.

Schott, J., Berner, R.A. and Sjöberg, E.L. (1981) Mechanism of pyroxene and amphibole weathering – I. Experimental studies of iron-free minerals. *Geochimica et Cosmochimica Acta*, **45**, 2123–2135.

Sposito, G. (1984) *The Surface Chemistry of Soils*. Oxford University Press, Oxford, UK.

Stillings, L.L. and Brantley, S.L. (1995) Feldspar dissolution at 25ºC and pH 3: Reaction stoichiometry and pH effect of cations. *Geochimica et Cosmochimica Acta*, **59**, 1483–1496.

Taubald, T., Bauer, A., Schäfer, T., Geckeis, H., Satir, M. and Kim, J.I. (2000) Experimental investigation of the effect of high-pH solutions on the Opalinus Shale and the Hammerschmiede smectite. *Clay Minerals*, **35**, 515–524.

Tournassat, C., Neaman, A., Villieras, F., Bosbach, D. and Charlet, L. (2003) Nanomorphology of montmorillonite particles: estimation of the clay edge sorption site density by low-pressure gas adsorption and AFM observations. *American Mineralogist*, **88**, 1989–1995.

Zysset, M. and Schindler, P.W. (1996) The proton promoted dissolution kinetics of K-montmorillonite. *Geochimica et Cosmochimica Acta*, **60**, 921–931.

(*Received 7 June 2004; revised 19 November 2004; Ms. 924; A.E. Peter J. Heaney*)

https://doi.org/10.1346/CCMN.2005.0530204 Published online by Cambridge University Press